http://dx.doi.org/10.5012/bkcs.2013.34.9.2822

Micro-solid Oxide Fuel Cells with Yttria-stabilized Zirconia and Nanoporous Pt Electrodes

Yun Tak Lim and Jong Yeog Son[†,*]

Department of Materials Science and Engineering, Pohang University of Science and Technology (POSTECH), Pohang 790-784, Korea
[†]*Department of Applied Physics, College of Applied Science, Kyung Hee University, Suwon 446-701, Korea*
[*]*E-mail: jyson@khu.ac.kr*
Received March 26, 2013, Accepted June 22, 2013

Key Words : Micro-solid oxide fuel cell, YSZ, Anodizing aluminum oxide (AAO), Nanoporous Pt electrodes

The emergence of portable electronic devices such as laptops, electronic books, and mobile phones has prompted a flurry of potential for the next generation of devices.[1-3] In particular, a miniaturized fuel cell is a promising power source for portable electronics. Recent studies have mainly investigated three types of micro-sized fuel cells[4-11]: a micro-polymer electrolyte/proton exchange membrane fuel cell (PEMFC), a micro-direct methanol fuel cell (DMFC), and a micro-solid oxide fuel cell (μSOFC). Both the PEMFC and DMFC exhibit fuel cell performance with a power density of 130 (195) $mWcm^{-2}$ and 100 $mWcm^{-2}$ in air (in ambient oxygen), respectively, but the PEMFC is disadvantageous in that one must safely treat explosive hydrogen and oxygen gases. In contrast, the μSOFC may provide a safe way to use syngas from hydrocarbon fuel, where operation temperatures may range between 300 °C and 600 °C.[11]

Recent studies on μSOFCs have focused on their micro-structures, electrical or electrochemical properties, modeling, and fabrication.[12-18] In particular, U. P. Muecke *et al.* presented a μSOFC consisting of two Pt electrodes sandwiching a layer of yttria-stabilized zirconia (YSZ) on a glass ceramic substrate, which exhibited a maximum power density of about 150 $mWcm^{-2}$ at 550 °C.[11] In this study, we present a Pt/YSZ/Pt μSOFC, where the two Pt electrodes forming the anode and cathode have almost uniform nanopores and a YSZ layer serves as the electrolyte. The Pt/YSZ/Pt μSOFC was fabricated using deposition and etching techniques with anodic aluminum oxide (AAO) nanotemplates to form almost uniform nanopores on the Pt electrodes. The resulting fuel cell exhibited a maximum power density of about 90 $mWcm^{-2}$ at 550 °C, which is less than that of the aforementioned previous result.

Experimental

Figure 1 presents schematics of the fabrication process of a μSOFC. Figure 1(a) shows a 40-μm-thick AAO nanotemplate with a diameter of 20 mm that was prepared as a bottom supporter; the mean pore diameter and pore-to-pore distance of the AAO nanotemplate are 30 nm and 100 nm, respectively. The AAO nanotemplate was made by employing a four-stage anodization technique on an Al sheet with a thickness of about 500 μm.[19] The four anodization processes were carried out in 0.3 M oxalic acid with a voltage of 40 V for 6, 10, 6, and 10 min, respectively, at 15 °C to form an almost uniform AAO nanotemplate. Then, 0.4 M chromic acid was used for 12 min at 65 °C to completely remove the Al_2O_3 layer formed on the surface of the Al film. An AAO nanotemplate, an upper Pt electrode, a YSZ electrolyte film, and a lower Pt electrode were serially deposited onto the bottom AAO nanotemplate, as shown in Figure 1(b).

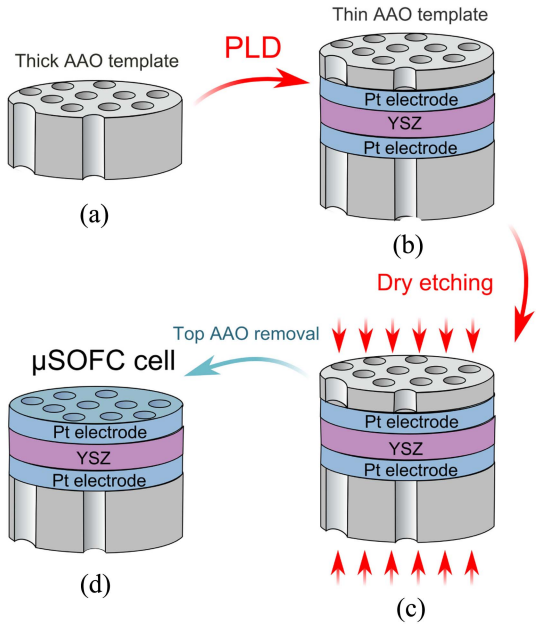

Figure 1. Schematic fabrication process of micro-solid oxide fuel cells (μSOFCs). (a) A thick AAO template is prepared. (b) A thin AAO nanotemplate, an upper Pt electrode, a yttria-stabilized zirconia (YSZ) film, and a lower Pt electrode are serially deposited on the thick AAO template. (c) Nanopores are formed on the upper and the lower Pt electrodes using dry etching techniques. (d) A μSOFC is formed after removing the top (thin) AAO nanotemplate.

More specifically, the lower Pt electrode was first deposited onto the bottom AAO nanotemplate with a thickness of 300 nm to form the cathode. Next, the YSZ layer was deposited

onto the lower Pt electrode with a thickness of 1500 nm via pulsed laser deposition (PLD); a commercially available 1-inch-diameter YSZ (Zr: 8%) target (Cerectron, South Korea) was used. In addition, a frequency-tripled Nd:YAG laser (λ = 355 nm) with a power of about 2 Jcm^{-2} was used at a target-to-substrate distance of 5 cm. Note that the base pressure, growth temperature, and oxygen partial pressure for the PLD depositon were about 5×10^{-7} Torr, 700 °C, and 100 mTorr, respectively. Following the YSZ deposition, the upper Pt electrode was deposited onto the YSZ film with a thickness of 300 nm to form the anode. Finally, a 1.6-μm-thick Al film was deposited on the upper Pt electrode. The Al film was anodized using the aforementioned four-stage anodization technique, resulting in a 400-nm-thick AAO nanotemplate with a mean pore diameter of 30 nm and a pore-to-pore distance of 100 nm.

Figure 1(c) shows the dry etching process that formed the nanopores of the upper and lower Pt electrodes through the top and bottom AAO nanotemplates, respectively. After the nanopores were formed on surface of the Pt electrodes, the top AAO nanotemplate was completely removed by perchloric acid diluted with an ethanol solution (ratio of 1:4 in volume) at 30 °C. Note that the bottom AAO nanotemplate and the Pt electrodes remained after etching the top 400-nm-thick AAO nanotemplate because the bottom AAO nanotemplate – with a thickness of 40 μm – and the Pt electrodes – with a thickness of 300 nm – were robust to the AAO remover for the given etching time. Figure 1(d) shows the Pt/YSZ/Pt μSOFC on the bottom AAO nanotemplate, where the two Pt electrodes have almost uniform nanopores. Note that a silver nitrate solution was used to electrically connect the upper and lower Pt electrodes with extension wires to form the anode and cathode, respectively. The silver nitrate solution was dried completely for 1 h at 100 °C to ensure a stable electrical connection.

Results and Discussion

Figure 2 shows scanning electron microscopy (SEM) images of the μSOFC. Figure 2(a) shows the side view of the YSZ/Pt/AAO structures, found in the lower part of the μSOFC, at an angle of about 10°. Almost uniform nanopores were formed in the AAO nanotemplate in this region. Figure 2(b) shows top view of the YSZ/Pt structure, found in the upper part of the μSOFC; a dotted line indicates the boundary between the YSZ film and the upper Pt electrode. We confirm that nearly uniform nanopores were formed in the upper Pt electrode after the dry etching described in Figure 1(c). Note that the left part of the upper Pt electrode in the window was removed to observe the surface morphology of the YSZ film.

Figure 3 shows the voltage (left vertical axis: filled symbols) and power density (right vertical axis: open symbols) of the μSOFC as a function of current density at temperatures of 450 °C (triangle), 500 °C (square), and 550 °C (circle), respectively. The power density, defined by the current density multiplied by the voltage, increases with the increasing temperature. Since the power density is proportional to the electrochemical reaction rate, we estimate the activation energy E_{AC} to be approximately 495 meV using the Arrhenius law – *i.e.* the electrochemical reaction rate ~exp($-E_{AC}/kT$), where k is the Boltzmann constant and T is an absolute temperature.

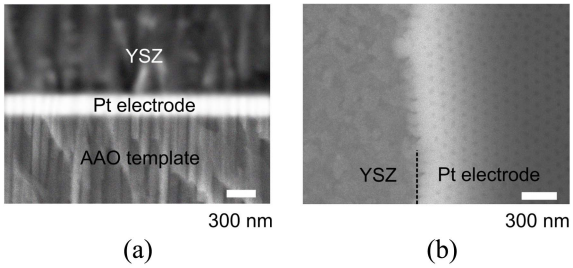

Figure 2. SEM images of a μSOFC: (a) Side view of a YSZ/Pt/AAO nanotemplate structure at an angle of 10°. (b) Top view of the YSZ/Pt electrode. The dotted line indicates the boundary between the YSZ film and the upper Pt electrode; the left part of the upper Pt electrode was removed to observe the YSZ layer.

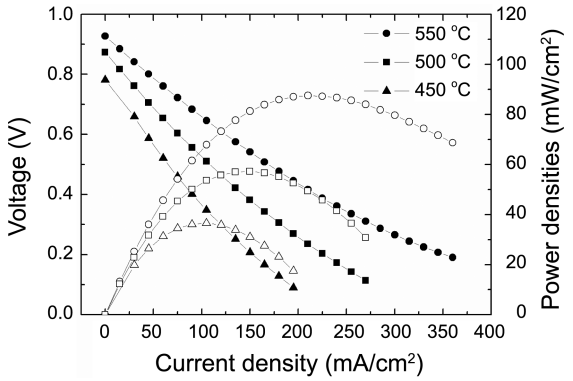

Figure 3. Current-voltage (left vertical axis) curve of the μSOFC with power densities (right vertical axis) at various temperatures, where the triangle, square, and circle symbols indicate the voltage (filled symbol) and power density (open symbol) at 450 °C, 500 °C, and 550 °C, respectively.

Note that the upper Pt electrode acts as an anode but is permeable to hydrogen gas and the lower Pt electrode acts as a cathode but is also effective for oxygen gas because the electrochemical reactions are confined to the vinicity of the triple phase boundary of the metallic Pt electrode.[20,21] The maximum power density in the μSOFC in this study was about 90 $mWcm^{-2}$, which may be comparable to or less than that found in the previously reported result as a high record.[11] We postulate that the nanopores in the μSOFC Pt electrodes act as channels to effectively migrate reactant gases such as H_2 and O_2 into the YSZ electrolyte. Interestingly, the bottom AAO nanotemplate acts as a cell supporter and is useful for the μSOFC because it is robust at temperatures up to 1000 °C.

Conclusion

We investigated a Pt/YSZ/Pt μSOFC by fabricating one using two AAO nanotemplates in conjuction with deposition

and etching techniques. The μSOFC exhibited a maximum power density of about 90 $mWcm^{-2}$ at 550 °C which is comparable to or less than the previously reported results as a high record. This study demonstrated that the nanoporous Pt electrodes and bottom AAO nanotemplate of the Pt/YSZ/Pt μSOFC produce a stable and efficient fuel cell performance at temperatures up to 550 °C.

References

1. (a) Nikbin, D. *Fuel Cell Review* **2006**, *3*, 21. (b) Tem, C.; Whitesides, G. M. *J. Am. Chem. Soc.* **1990**, *112*, 6409.
2. Maynard, H. L.; Meyers, J. P. *J. Vac. Sci. Technol.* **2002**, *B 20*, 1287.
3. Dyer, C. K. *J. Power Sources* **2002**, *106*, 31.
4. Wong, C. W.; Zhao, T. S.; Ye, Q.; Liu, J. G. *J. Power Sources* **2006**, *155*, A1600.
5. Modroukas, D.; Modi, V.; Frechette, L. G. *J. Micromech. Microeng.* **2005**, *15*, S193.
6. Lu, G. Q.; Wang, C. Y. *J. Power Sources* **2005**, *144*, 141.
7. Morse, J. D. *Int. J. Energy Res.* **2007**, *31*, 576.
8. La O, G. J.; In, H. J.; Crumlin, E.; Barbastathis, G.; Shao-Horn, Y. *Int. J. Energy Res.* **2007**, *31*, 548.
9. Nguyen, N. T.; Chan, S. H. *J. Micromech. Microeng.* **2006**, *16*, R1.
10. Yu, J.; Cheng, P.; Ma, Z.; Yi, B. *J. Power Sources* **2003**, *124*, 40.
11. Muecke, U. P.; Beckel, D.; Bernard, A.; Bieberle-Hutter, A.; Graf, S.; Infortuna, A.; Muller, P.; Rupp, J. L. M.; Schneider, J.; Gauckler, L. J. *Adv. Funct. Mater.* **2008**, *18*, 3158.
12. Tsai, T.; Barnett, S. A. *J. Vac. Sci. Technol.* **1995**, *A 13*, 1073.
13. Rupp, J. L. M.; Gauckler, L. J. *Solid State Ionics* **2006**, *177*, 2513.
14. Beckel, D.; Muecke, U. P.; Gyger, T.; Florey, G.; Infortuna, A.; Gauckler, L. J. *Solid State Ionics* **2007**, *178*, 407.
15. Suzuki, T.; Kosacki, I.; Anderson, H. U. *Solid State Ionics* **2002**, *151*, 111.
16. Fleig, J.; Tuller, H. L.; Maier, J. *Solid State Ionics* **2004**, *174*, 261.
17. Huang, H.; Nakamura, M.; Su, P.; Fasching, R.; Saito, Y.; Prinz, F. B. *J. Electrochem. Soc.* **2007**, *154*, B20.
18. Chen, X.; Wu, N. J.; Smith, L.; Ignatiev, A. *Appl. Phys. Lett.* **2004**, *84*, 2700.
19. Kim, W.-H.; Park, S.-J.; Son, J.-Y.; Kim, H. *Nanotech.* **2008**, *19*, 045302.
20. Robertson, N. L.; Michaels, J. N. *J. Electrochem. Soc.* **1990**, *137*, 129.
21. Baker, R.; Guindet, J.; Kleitz, M. *J. Electrochem. Soc.* **1997**, *44*, 2427.
22. Lim, Y. T.; Son, J. Y.; Baik, S. *Electrochemical and Solid-State Letters* **2010**, *13*, B117.
23. Lim, Y. T.; Son, J. Y. *Electron. Mater. Lett.* **2013**, *9*, 241.